Structure and Kinetics of Formation of Catechol Complexes of Ferric Soybean Lipoxygenase-1†

Mark J. Nelson,*,‡ Bridget A. Brennan,‡ D. Bruce Chase,‡ Rebecca A. Cowling,‡ Geoffrey N. Grove,§ and Robert C. Scarrow*,§

Central Research and Development, E. I. du Pont de Nemours & Co., Wilmington, Delaware 19880-0328, and Department of Chemistry, Haverford College, Haverford, Pennsylvania 19041

Received June 12, 1995; Revised Manuscript Received August 21, 1995⊗

ABSTRACT: Ferric soybean lipoxygenase forms stable complexes with 4-substituted catechols. The structure of the complex between the enzyme and 3,4-dihydroxybenzonitrile has been studied by resonance Raman, electron paramagnetic resonance, visible, and X-ray spectroscopies. It is a bidentate iron−catecholate complex with at least one water ligand. The kinetics of formation of complexes between lipoxygenase and 3,4-dihydroxybenzonitrile and 3,4-dihydroxyacetophenone have been studied by stopped-flow spectroscopy. The data are consistent with two kinetically distinct, reversible steps. The pH dependence of the first step suggests that the substrate for the reaction is the catechol monoanion. When these results are combined, plausible mechanisms for the complexation reaction are suggested.

Soybean lipoxygenase isozyme 1 is a non-heme iron enzyme that catalyzes the addition of dioxygen to linoleic acid, yielding (13*S*)-9,11(*Z*,*E*)-octadecadienoic acid (13(S)-HPOD[1]) as the dominant product at pH 9 (Gardner, 1991; Siedow, 1991). This enzyme stands in contrast to the other mononuclear non-heme iron oxygenases (e.g., proline hydroxylase, catechol dioxygenases, and isopenicillin N synthase) in that the O−O bond is not cleaved during the reaction. The metal ion in the non-heme iron oxygenases appears to be intimately involved in catalysis; consequently, the uniqueness of the lipoxygenase reaction presumably results in large part from differences in the reactivity of its iron site. A model for the iron site in active, ferric lipoxygenase (SLO^A) is shown in Figure 1. The identities of the histidine, carboxylate, and asparagine ligands are derived from the crystal structure of ferrous lipoxygenase (Boyington et al., 1993; Minor et al., 1993), the existence

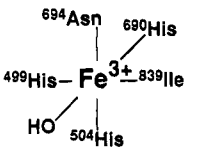

FIGURE 1: Model for the structure of the iron site in ferric lipoxygenase (Scarrow et al., 1994). ^{694}Asn is an O donor carboxamide ligand, and ^{839}Ile is the C-terminal residue of the protein and is coordinated via its carboxylate.

of the hydroxide ligand from EPR and EXAFS spectroscopies (Nelson, 1988b; Scarrow et al., 1994), and the overall coordination number from XANES (Van der Heijdt et al., 1992; Scarrow et al., 1994), CD, and MCD spectroscopies (Zhang et al., 1991).

The mechanisms proposed for the lipoxygenase dioxygenase reaction depend on the ability of the metal ion to participate in redox chemistry and to coordinate substrates, intermediates, or products of the reaction. In one mechanism, the role of the iron is to oxidize the substrate to a radical species that adds dioxygen directly (De Groot et al., 1975). This requires a reduction potential for Fe^{3+} that is unusually high for a non-heme iron enzyme. In fact, ferric lipoxygenase has been demonstrated to oxidize linoleic acid in the absence of dioxygen, consistent with this mechanism (De Groot et al., 1975).

In a second proposed mechanism, the role of the ferric ion is to form a σ-organoiron complex with the substrate, and dioxygen inserts into the Fe−C bond (Corey & Nagata, 1987). The ferric ion in SLO^A is six-coordinate (Zhang et al., 1991; Van der Heijdt et al., 1992; Scarrow et al., 1994); therefore, this requires either a seven-coordinate intermediate or that ligand exchange reactions occur at a rate at least comparable to the rate of catalysis (approximately 300 s^{-1} at 25 °C). Several exogenous ligands (azide, thiocyanate, and catechols) will coordinate the iron (Galpin et al., 1976; Cox et al., 1988; Zhang et al., 1991; Gaffney et al., 1993), but the rates of these reactions and the structures of the resulting complexes have not been reported.

† Research at Haverford College is supported by American Chemical Society Petroleum Research Fund Grant 21967-GB3, NIH Grant GM51045-01, and the Undergraduate Biological Sciences Education Initiative of the Howard Hughes Medical Institute. X-ray data were collected at the National Synchrotron Light Source, Brookhaven National Laboratory, which is supported by the U.S. Department of Energy, Divisions of Materials Science and Chemical Science (DOE Contract no. DE-AC02-76CH00016).

* To whom correspondence should be addressed.

‡ DuPont. Contribution 7031 from Central Research and Development.

§ Haverford College.

⊗ Abstract published in *Advance ACS Abstracts,* November 1, 1995.

[1] Abbreviations: 13(S)-HPOD, (13*S*)-9,11(*Z*,*E*)-octadecadienoic acid; BisTris, 2-[bis(2-hydroxyethyl)amino]-2-(hydroxymethyl)-1,3-propanediol; BVS, bond valence sum; catH, catechol monoanion; DBC, 3,5-di-*tert*-butylcatechol; DHAP, 3,4-dihydroxyacetophenone; DHBA, 3,4-dihydroxybenzaldehyde; DHBN, 3,4-dihydroxybenzonitrile; EXAFS, extended X-ray absorption fine structure; GOF, goodness of fit; NSLS, National Synchrotron Light Source, Brookhaven National Laboratory; NTB, tris(benzimidazol-2-ylmethyl)amine; R2 DOPA-208, ribonucleotide reductase with dopamine at the β-208 position; salen, ethylenebis(salicylimine) dianion; SLO^A, ferric soybean lipoxygenase isozyme 1; SLO^A·DHAP, the complex between SLO^A and DHAP; SLO^A·DHBN, the complex between SLO^A and DHBN; TFMC, 3,4-dihydroxy-α,α,α-trifluorotoluene; TPA, tris(2-pyridylmethyl)amine; XANES, x-ray absorption near edge spectroscopy.

0006-2960/95/0434-15219$09.00/0

We investigated the ability of the metal ion in SLO^A to undergo ligand exchange reactions and expansion of its coordination sphere using 3,4-dihydroxybenzonitrile (DHBN) and 3,4-dihydroxyacetophenone (DHAP) as probes of the metal site. Catechols have been used previously to probe metal ion coordination in a variety of non-heme iron enzymes, including lipoxygenase (Galpin et al., 1976; Que & Epstein, 1981; Cox et al., 1988; True et al., 1990; Michaud-Soret et al., 1995). We report stopped-flow visible spectroscopy of complex formation as well as EPR, X-ray absorption, visible, and resonance Raman spectra of the species obtained. In its complex with the active site iron, DHBN supplies two of the six ligands to the metal ion, requiring exchange of two of the endogenous ligands during the complexation reaction.

The kinetics of complex formation are consistent with a two-step reaction, with both steps much slower than the dioxygenase reaction. EPR spectra of samples prepared with saturating amounts of DHBN or DHAP exhibit a previously unreported feature at $g = 8.1$ that may be an intermediate of the complexation reaction.

MATERIALS AND METHODS

Pyrocatechol, 3,4-dihydroxybenzaldehyde (DHBA), and $H_2{}^{18}O$ (95%-enriched) were obtained from Aldrich Chemical Co. and DHBN and DHAP from Pfaltz and Bauer. $H_2{}^{17}O$ (50%-enriched) was obtained from Cambridge Isotopes. The catechols were used without further purification. Tris(benzimidazol-2-ylmethyl)amine (NTB) and its Fe^{3+} complex were synthesized as previously reported (Thompson et al., 1977; Cox et al., 1988). Lipoxygenase and 13(S)-HPOD were prepared as previously described (Nelson et al., 1994). Samples of SLO^A were exchanged into $H_2{}^{17}O$ or $H_2{}^{18}O$ by lyophilization, followed by reconstitution in the isotopically enriched water. The pH of these samples was within 0.05 unit of the pH of controls reconstituted with natural abundance water.

3,4-Dihydroxy-α,α,α-trifluorotoluene (TFMC). 2-Nitro-4-(trifluoromethyl)phenol (1 g) dissolved in ethanol (20 mL) was hydrogenated in a Parr device using Raney nickel as catalyst. The solution was filtered to remove solids (**CAUTION**! Raney nickel is pyrophoric when dry; care must be taken to keep the filtered solids moist). The solution was evaporated to dryness, yielding the crude amine as a yellow powder. The catechol was synthesized without isolation of the intermediate diazonium ion (Cohen et al., 1977). The crude 2-amino-4-(trifluoromethyl)phenol was dissolved in 10 mL of 35% (v/v) concentrated sulfuric acid at 0 °C. Sodium nitrite (0.35 g in 2 mL of water) was added slowly and the solution allowed to stir on ice for 10 min. Two crystals (approximately 15 mg) of urea were added to quench excess nitrite, and then $Cu(NO_3)\cdot 3H_2O$ (19 g in 175 mL of water) and solid Cu_2O (0.7 g) were added. This green solution was extracted with ether, and the ether layer was washed with water, dried with sodium sulfate, and evaporated to an oil. The crude 3,4-dihydroxy-α,α,α-trifluorotoluene was purified by dissolving it in CH_2Cl_2 and extracting it into an aqueous solution of $FeCl_3$. The purple $Fe^{3+}(TFMC)_3$ solution was titrated with 1 M HCl until it turned blue, and the neutral catechol was extracted into CH_2Cl_2. This solution was dried over sodium sulfate and evaporated to an oil. The product was homogeneous by TLC (silica gel, 1:1 CH_2Cl_2/ether) and showed an NMR spectrum (acetone-d_6) with a multiplet at δ 6.9 (3 protons) and a broad singlet at δ 8.5 (1.7 protons). The presence of a small water peak in the spectrum suggests that the low integration of the phenolic protons resulted from exchange with water.

Stopped-Flow Visible Spectroscopy. The as-isolated (ferrous) enzyme was oxidized by addition of 13(S)-HPOD until the first appearance of absorption at 585 nm indicated the oxidation was complete. The sample of SLO^A was divided into aliquots which were dialyzed into either 0.1 M potassium phosphate (pH 7.5 and below) or 0.05 M potassium pyrophosphate (pH 7.8 and above) buffer. Enough NaCl was added to each buffer to bring the calculated ionic strength to 0.5 M. After dialysis, the pH of the enzyme samples was verified and the concentration of protein estimated from the absorbance at 280 nm; this was approximately 10 mg/mL. An aliquot was taken for subsequent colorimetric iron determination. Solutions of catechols were prepared in the same buffers.

Data were obtained using an OLIS stopped-flow spectrophotometer interfaced to a Zenith personal computer (PC). The syringes and mixing chamber were immersed in a thermostated water bath held at 15 °C. Equal volumes of the enzyme and catechol solutions were mixed, and the evolution of absorbance at the maximum of the catechol-to-iron charge transfer band was followed. The data (voltage vs time) were fitted (using Asystant running on an IBM PC/XT) with eq 6, modified to reflect the fact that $A = \log(V_0/V)$; V_0, the voltage when $A = 0$, was obtained from the fitting procedure.

Dissociation Rates. Samples of SLO^A, prepared as above except in deoxygenated buffer, were placed in a serum-stoppered cuvette in the thermostated (15 °C) cuvette holder of an HP 8451a diode array spectrophotometer. A substoichiometric amount of DHBN or DHAP was added, and the visible spectrum was followed until equilibrium. Then a 100-fold excess of pyrocatechol (in the same deoxygenated buffer) was added by syringe, and the spectrum was followed as a function of time. The absorbances at 350 nm and at the peak of the long wavelength catechol-to-iron charge transfer band were extracted and the data fitted with eq 10.

EPR Spectroscopy. EPR spectra were obtained using a Brucker EM-200 spectrometer with an Oxford Instruments ESR900 liquid helium cryostat. The conditions were as follows: microwave frequency, 9.4 GHz; modulation amplitude, 1.0 mT; microwave power, 10 mW; T, 5 K; and scan rate, 0.45 mT/s. The temperature was verified at intervals during the experiment both by use of an AuFe/chromel thermocouple in a dummy EPR tube and by comparison of the intensity of the spectrum of a standard sample of $Cu^{2+}(acac)_2$ at the temperature of the experiment to that at the base temperature of liquid helium.

Resonance Raman Spectroscopy. The sample was cooled with an Air Products LT3-110 cryostat using liquid N_2 as the refrigerant with a typical sample temperature of 80 K. Samples were loaded onto a precooled (270 K) gold-plated copper cold finger with wells for four 12 μL samples. The samples were frozen rapidly; Dewar evacuation was begun at a sample temperature of 200 K to minimize the possibility of lyophilization.

A Spectra-Physics 2040 Ar-ion laser was used at 514 nm to pump a Spectra-Physics 3900 Ti-sapphire laser, capable of producing several hundred milliwatts of tuneable radiation

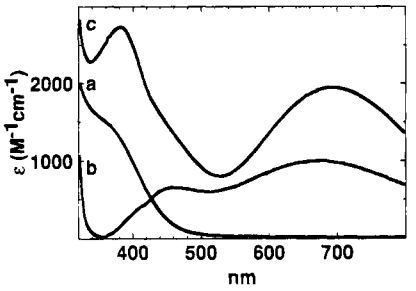

FIGURE 2: Visible spectra of (a) SLO^A (pH 7), (b) SLO^A·DHBN (pH 7.0), and (c) $[Fe(NTB)(CHBN)]^+$ (methanol).

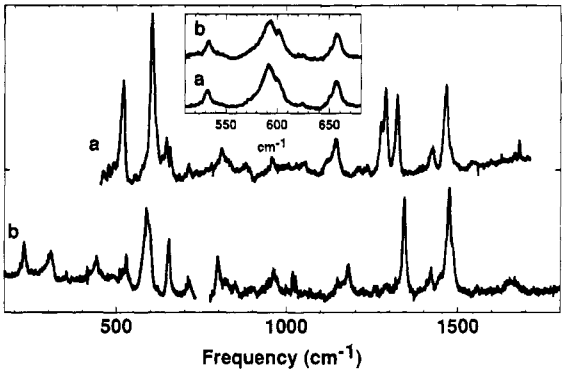

FIGURE 3: Resonance Raman spectra of (a) $[Fe(NTB)(DHBN)]^+$ (solid sample) and (b) SLO^A·DHBN at pH 7.0, both taken with 714 nm excitation. The inset is SLO^A lyophilized and redissolved in (a) 50%-enriched $H_2{}^{18}O$ or (b) natural abundance H_2O before addition of DHBN.

from 680 to 760 nm. The output of the Ti-sapphire laser was optically filtered to remove nonlasing emission using a double pass prism monochromator followed by a Newport Model 910 spatial filter. Power at the sample was typically 50 mW. Raman spectra were recorded in a 180° backscattering configuration using an f/1.3 camera lens for collection. The collected Raman scattered light was dispersed using a SPEX Model 1877 triplemate monochromator and detected with a Tektronix 1024×1024 thinned, backside-illuminated CCD element (peak quantum efficiency of 90% at 700 nm) mounted in a Photometrics CCD9000 detection system. The CCD was operated at −110 °C. The spectrometer was calibrated using the atomic emission lines from Ar, Kr, Ne, or Xe pen lamps. Spectral resolution was 4−6 cm^{-1}, corresponding to 5−7 pixels on the CCD. The data were processed and displayed using Labcalc (Galactic Industries).

XANES and EXAFS Spectroscopy. Samples of lipoxygenase were oxidized by addition of 13(S)-HPOD (*vide supra*), dialyzed into 0.05 M BisTris acetate (pH 7.0) (4 °C; pH 6.8, 25 °C), and concentrated by ultrafiltration in Amicon Centricon units. Two samples were prepared, each approximately 300 mg of protein/mL. DHBN (2 equiv) in buffer was added to one sample prior to the final concentration. The concentrated samples were frozen in sample holders and maintained at ca. 80 K for data collection.

Data were obtained at NSLS beam line X19a using a Si 220 monochromator and a 13-element Ge solid state detector (Canberra). Other details of data collection and analysis are as described previously (Scarrow et al., 1994).

RESULTS

Structure of Lipoxygenase−Catechol Complexes. Solutions of native SLO^A are faintly yellow as the result of absorbance at approximately 350 nm, assigned to an imidazole-to-Fe^{3+} ligand-to-metal charge transfer transition (Zhang et al., 1991) (Figure 2a). Upon addition of a 4-substituted catechol (e.g., DHBN), a blue to blue-green color slowly appears, and the visible spectrum changes to one characteristic of a ferric catecholate complex (Cox et al., 1988; Nelson, 1988a) (Figure 2b).

We used resonance Raman spectroscopy to characterize the structure of SLO^A·DHBN, with excitation into the lower energy band of the complex. The spectrum of a sample prepared at pH 7 is shown in Figure 3, along with the spectrum of $[Fe(NTB)(DHBN)]^+$. The features at 529, 589, 653, 796, 1148, 1178, 1341, 1420, and 1474 cm^{-1} in the SLO^A·DHBN spectrum are typical of bidentate ferric catecholate complexes of 4-substituted catechols (Table 1). The features below 700 cm^{-1} have been shown to be associated with Fe−O vibrations on the basis of ^{18}O isotope effects (Michaud-Soret et al., 1995). The feature at 529 cm^{-1} has been assigned as an iron−catechol chelate ring mode and is found between 511 and 526 cm^{-1} in spectra of a number of monoferric complexes with tetradentate ligands and one bidentate catechol (Pyrz et al., 1985; Cox et al., 1988). In contrast, this feature is not found in the spectrum of the monodentate catecholate species Fe(salen)catH (Pyrz et al., 1985); its presence is therefore diagnostic of a bidentate iron−catechol complex. The features near 589 and 653 cm^{-1} in the spectrum of SLO^A·DHBN are associated with the interactions between the iron and the oxygens at C-3 and C-4 of the catechol, respectively (Michaud-Soret et al., 1995). Note that the energy of the Fe−O(C-4) stretch in Fe(NTB)−catechol complexes depends on the identity of the catechol substituent, with more electron-withdrawing species giving rise to higher energy Fe−O vibrations. From the number and energies of the features in the 500−700 cm^{-1} region of the spectrum, we conclude that the catechol in SLO^A·DHBN exists as a bidentate ligand to the ferric ion.

No rigorous assignment of the higher energy features has been made in other systems, but the effects of ring deuteration suggest that they have substantial C−H bending and C=C stretching character (Pyrz et al., 1985; Michaud-Soret et al., 1995). Most of these features are seen in both spectra in Figure 3; however, the peaks at 1287 and 1544 cm^{-1} in the spectrum of $[Fe(NTB)(DHBN)]^+$ are weak or absent in the SLO^A·DHBN spectrum obtained with 714 nm excitation. These two features have been shown to be more strongly resonance-enhanced with higher energy excitation (Cox et al., 1988), and peaks at 1296 and 1556 cm^{-1} were observed in spectra of SLO^A·DHBN taken with 612 nm excitation (data not shown). The requirement of higher energy excitation to observe these bands in the spectrum of SLO^A·DHBN is consistent with the higher energy of the ligand-to-metal charge transfer bands in SLO^A·DHBN as compared to $[Fe(NTB)(DHBN)]^+$ (Figure 2c). Finally, there is a feature at 1420 cm^{-1} in both spectra in Figure 3 that is not found in spectra of ferric complexes of unsubstituted catecholates; however, this feature is seen in spectra of other complexes of 4-substituted catecholates (Table 1) and therefore presumably arises from the lowered symmetry of the iron−catechol unit.

The low-field region of the EPR spectra of SLO^A·DHBN is substantially different from that of SLO^A (Figure 4) (Nelson, 1988). EPR spectra of high-spin ferric complexes

Table 1: Positions of the Major Features in the Resonance Raman Spectra of Iron–Catechol Complexes

	λ_{ex} (nm)	Raman vibrations (cm^{-1})											reference
model complexes													
$[Fe(cat)_3]^{3-}$ [a]	496.1	533		621	800	1154	1262	1322		1487	1572		Salama et al., 1978
$[Fe(salen)(cat)]^{3-}$ [b]	647.1	511		614	796	1145	1260	1324		1487			Pyrz et al., 1985
$[Fe(NTB)(cat)]^{+}$ [c]	605.1	518		630	828	1148	1248	1302		1454	1570		Cox et al., 1988
$[Fe(NTB)(DHBN)]^{+}$ [d]	714	521	603	646	806	1142	1275 1287	1321	1424	1465	1544		this work
$[Fe(NTB)(DHBA)]^{+}$ [d]	714	512 529	570	614 649	818	1149	1279	1321	1431	1463			this work
$[Fe(NTB)(DHAP)]^{+}$ [d]	714	517	558	616	808	1185 1200	1284	1319	1416	1466			this work
proteins													
phenylalanine hydroxylase + cat[e]	620.5	531		621		1151	1257	1313		1470	1568		Cox et al., 1988
tyrosine hydroxylase + dopamine[e]	606	528	592	631	814		1275	1320	1425	1475			Michaud-Soret et al., 1995
R2 DOPA-208[f]	676.4	512	592	619	806	1143	1263	1319	1350	1475	1569		Ormö et al., 1992
R2 [3-^{18}O]DOPA-208[f]	676.4	499	584	617		1143	1263	1319	1350	1475	1569		Ling et al., 1994
lipoxygenase + DHBN[f]	719	529	589	653	796	1148 1178		1341	1420	1474			this work
lipoxygenase + DHBA[e]	612	576	620	648	760			1338	1444	1488			this work
lipoxygenase + DHAP[e]	612	538	610	642	762		1296	1334	1448	1492	1554		this work

[a] H_2O, ambient temperature. [b] CD_3CN, ambient temperature. [c] CD_3OD, ambient temperature. [d] Solid, ambient temperature. [e] 4 °C. [f] 90 K.

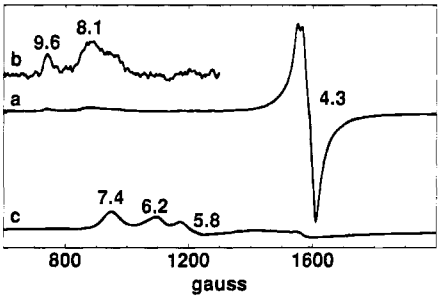

FIGURE 4: EPR spectra of SLO^A. (a) SLO^A·DHBN, pH 7.5. (b) Part a × 10. (c) SLO^A, pH 7.5.

are interpreted using the spin Hamiltonian (Pilbrow, 1990)

$$\hat{H}_e = g_0\beta_e S\cdot H + D[S^2_z - {}^{35}/_{12} + E/D(S^2_x - S^2_y)] \quad (1)$$

where D and E/D are the zero-field splitting parameters. In a so-called proper coordinate system, E/D varies from 0 to $^1/_3$, reflecting axial and rhombic electronic symmetry of the iron at the extremes (Blumberg, 1967; Gaffney & Silverstone, 1993). The high-spin ferric ions in native SLO^A show two primary EPR signals in this region (Figure 4c), one with $g' \approx 7.4$ and one with $g' \approx 6.2$ and 5.8 (Slappendel et al., 1981; Gaffney et al., 1993), reflecting a nearly axial electronic environment [$E/D = 0.065$ and 0.015, respectively (Gaffney et al., 1993)]. Spectra of SLO^A·DHBN show signals at $g' \approx 9.6$ and 4.3 from the lowest and middle energy Kramers' doublets of an $S = {}^5/_2$ system with $E/D \approx 0.32$ (Figure 4a,b).

The EPR spectra of the SLO^A–catechol solutions also show features at $g' \approx 8.1$ and 5.5 that are not present in spectra of the uncomplexed enzyme and that have not been previously reported for lipoxygenase (Figure 4b). These features correspond to transitions in the lower and middle doublets of an $S = {}^5/_2$ system with $E/D \approx 0.10$. The intensity of the $g' \approx 8.1$ feature varies with pH; in spectra of SLO^A·DHBN (prepared with saturating amounts of DHBN), it is most intense at pH 7.5 and less intense at both lower and higher pH. Comparison of the intensity of the $g' \approx 8.1$ signal in spectra of SLO^A·DHBN to that of the $g' \approx 7.4$ and 6.2 signals in spectra of SLO^A suggests that about 20% of the SLO^A·DHBN complex exists in this form at equilibrium at pH 7.5 and about 10% at pH 6.9 and 8.1.

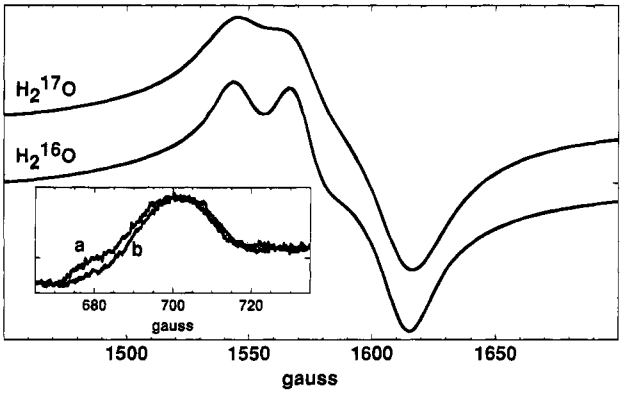

FIGURE 5: EPR spectra of SLO^A·DHBN at pH 7.0. The inset is the $g = 9.6$ feature arising from the ground state Kramers' doublet. (a) SLO^A lyophilized and redissolved in 50%-enriched $H_2{}^{17}O$ before addition of DHBN. (b) SLO^A lyophilized and redissolved in natural abundance H_2O before addition of DHBN.

Figure 5 shows EPR spectra of SLO^A·DHBN prepared using protein lyophilized and redissolved in either natural abundance water or 50%-enriched $H_2{}^{17}O$. The line broadening seen in both the $g \approx 4.3$ and $g \approx 9.6$ features in the spectrum of the latter sample demonstrates the presence of at least one oxygen derived from water as a ligand to the metal ion. That oxygen could be a water or hydroxide ligand, or it could be present as one of the catecholate oxygens following a lipoxygenase-catalyzed exchange of ^{17}O between water and the catechol hydroxyls.

Oxygen exchange between water and catechols occurs under very acidic conditions (Clay & Murphy, 1980). However, the exchange between water and semiquinones is more facile (Stevenson et al., 1988), and transient semiquinone species could result from reversible redox reactions in SLO^A–catechol solutions. To test the possibility of oxygen isotope exchange in the catechol ligand, we prepared a sample of SLO^A lyophilized and redissolved in 95%-enriched $H_2{}^{18}O$ and then treated with DHBN in the same way the $H_2{}^{17}O$-enriched EPR samples were prepared. The resonance Raman spectra of SLO^A·DHBN prepared in $H_2{}^{16}O$ and $H_2{}^{18}O$ are virtually identical; in particular, the 529, 589, and 653 cm^{-1} peaks that arise from Fe–O vibrations move less than 1 cm^{-1} upon substitution of $H_2{}^{18}O$ for $H_2{}^{16}O$ (Figure

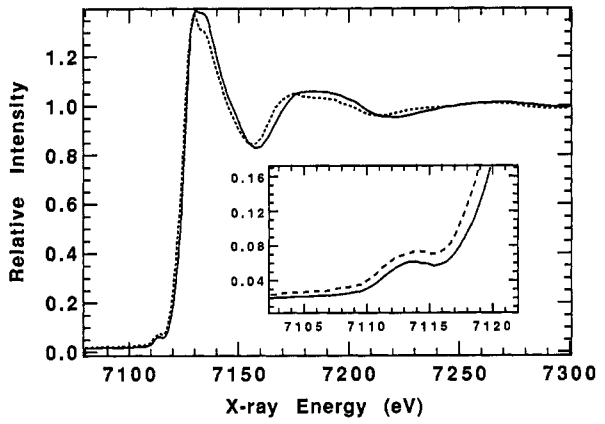

FIGURE 6: Base line-corrected and edge-normalized X-ray fluorescence spectra of SLO^A (- - -) and SLO^A·DHBN (—), each frozen at pH 7. The inset is an expansion of the 1s → 3d pre-edge peaks.

3, inset). Studies of tyrosine hydroxylase with ^{18}O-enriched dopamine coordinated to the iron (Michaud-Soret et al., 1995) demonstrated substantial shifts in these peaks when ^{18}O was incorporated into the catechol. The feature at 592 cm^{-1} [assigned to the Fe−O(C-3) interaction] shifts 12 cm^{-1} upon enrichment with ^{18}O at the C-3 oxygen. The feature at 631 cm^{-1} [assigned to the Fe−O(C-4) interaction] shifts 12 cm^{-1} upon substitution of both the C-3 and C-4 oxygens. In the case of the ferric DOPA complex in ribonucleotide reductase R2 (F208Y), the 529 cm^{-1} peak shifts 13 cm^{-1} upon ^{18}O substitution of the C-3 catecholate oxygen (Ling et al., 1994). The lack of significant shifts in any of the features assigned to Fe−O interactions in SLO^A·DHBN in $H_2{}^{18}O$ demonstrates that significant exchange of solvent water into the catecholate oxygens of the complex does not occur under these conditions. In turn, that allows us to conclude that the ^{17}O line broadening observed in the EPR spectrum arises from either a $Fe^{3+}-OH_2$ or $Fe^{3+}-OH^-$ bond.

Figure 6 compares the X-ray fluorescence spectrum of SLO^A·DHBN to that of SLO^A. The integrated intensities for the pre-edge feature, assigned to the 1s → 3d bound-state transition, are 6 ± 2 units (electron volts·percent edge height) for SLO^A and 5 ± 2 units for SLO^A·DHBN. These overlap with the range (6−9 units) found for crystallographically characterized pseudo-octahedral six-coordinate ferric complexes. Less centrosymmetric five- or four-coordinate complexes have pre-edge peaks that are at least twice as large (Roe et al., 1984). However, a small pre-edge peak is also observed for seven-coordinate complexes. Consequently, the XANES data for SLO^A·DHBN imply a coordination number for iron of six or seven.

A comparison of the EXAFS data for SLO^A and SLO^A·DHBN is shown in Figure 7, along with the best fits to the data. The first sphere EXAFS of SLO^A is fit well by a two-shell model, but not by a single shell model (Table 2 and Figure 7a) (Scarrow et al., 1994). The bond valence sum (BVS) for the two-shell fit in Table 2 (fit A2) is within 0.25 of the oxidation state of the ferric ion, as expected for an accurate fit (Thorpe, 1992).[2] The shorter shell in SLO^A has

[2] BVS values (Brown & Altermatt, 1985) are calculated using r_0(Fe−O) = 1.759 Å and r_0(Fe−N) = 1.831 Å. The average BVS for 41 high-spin ferric model complexes with only Fe−O and Fe−N bonds is 3.06, with a standard deviation of ±0.09 and a range of 2.84−3.25 (Scarrow et al., 1994).

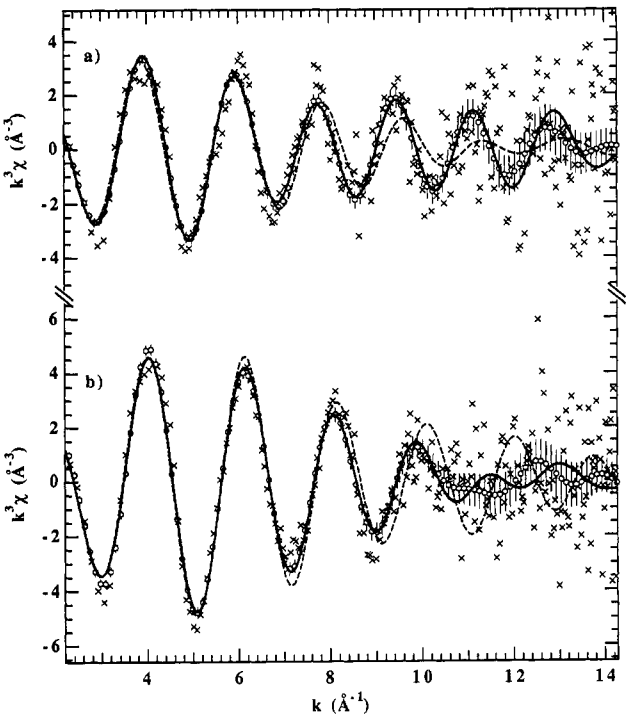

FIGURE 7: EXAFS (×) of (a) ferric lipoxygenase and (b) its DHBN complex. Vertical lines from the Fourier-filtered data (○) indicate σ_d (footnote *c*, Table 2). Solid curves are fits A2 and D6 (Table 2); dashed curves are fit A1 and a fit (R^2 = 3.4) assuming 4 O at 1.993 Å and 2 N at 2.16 Å ($\Delta\sigma^2 \equiv 0$).

Table 2: Fits to EXAFS of SLO^A and SLO^A·DHBN[a]

fit[b]	*n* & atom	*r* (Å)	$\Delta\sigma^2$ (Å^2)	*R*[c]	GOF[d]	BVS
A1	5.4 N	2.097	0.005_4[e]	2.52	1.89	
A2	1O	1.886	0[f]	0.24	0.58	2.94
	2O & 3 N	2.104_0	0.0016			
D1	7.2 N	2.042	0.0048	1.05	1.22	
D2	6.1 O	2.015_8	0.0065	0.65	0.96	
D3	4 O & 3N	2.025_0	0.0066	0.77	0.98	3.72
D4	3 O & 3 N	2.027	0.0042	0.97	1.10	3.22
D5	4 O & 2 N	2.022_8	0.0049	0.77	0.98	3.15
D6	2O	1.940	0[f]	0.82	1.01	3.11
	2 O & 2 N	2.075	0[f]			
		2.030[g]	*0.0041*			
D7	1 O	1.91_6	0[f]	0.87	1.11	3.08
	2 O	1.996	0[f]			
	1 O & 2 N	2.097	0[f]			
		2.033	*0.0048*			

[a] Fourier-filtered (FT 1.0−14.3 Å^{-1}; BT 1.0−2.3 Å) $k^3\chi$ values are refined between k = 2.2 and 14.3 Å. [b] A: SLO^A, pH 7. D: SLO^A·DHBN complex. [c] The residual minimized is R = average $[k^3(\chi_{calc} - \chi_{obs})/\sigma_d]^2$; σ_d is the uncertainty in the data, interpolated from (k, σ_d) = (2.2, 0.14), (4, 0.19), (8, 0.26), (10, 0.42), (13, 0.88), and (14.3 Å^{-1}, 0.56 Å^{-3}) (Scarrow et al., 1994). [d] GOF = $[Rn_{ind}/(n_{ind} - n_{var})]^{1/2}$, where n_{ind} is the number of independent data after Fourier transformation (10.1) and n_{var} is the number of refined parameters. [e] The least squares estimated standard deviation of a subscripted last digit is between 3 and 6; otherwise, it is 1 or 2. [f] $\Delta\sigma^2 \equiv 0$. [g] Values in italics are mean and standard deviations of the refined bond lengths.

been interpreted as arising from a Fe−OH bond (Scarrow et al., 1994).

The EXAFS of SLO^A·DHBN can be fit well by a single scattering shell. Because *n* is generally determinable to within about 15%, and because the coordination sphere of the iron almost certainly contains both N and O ligands, the refined *n* of fits D1 and D2 indicate either six or seven coordination for the iron in SLO^A·DHBN. The BVS may

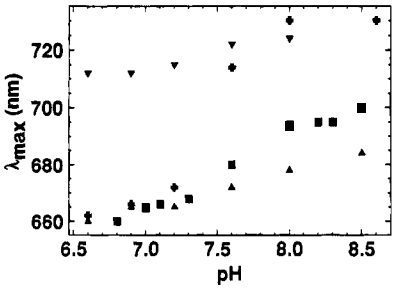

FIGURE 8: Maxima of the low-energy ligand-to-metal charge transfer band. (▼) SLO^A·TFMC. (+) SLO^A·DHBA. (■) SLO^A·DHAP. (▲) SLO^A·DHBN.

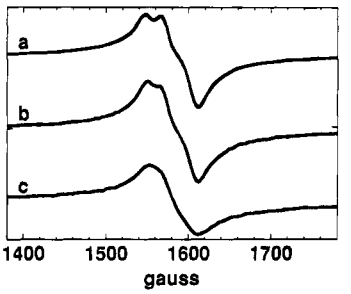

FIGURE 9: EPR spectra of SLO^A·DHBN. (a) pH 6.6 (intensity × 0.2) (b) pH 7.5 (c) pH 8.1.

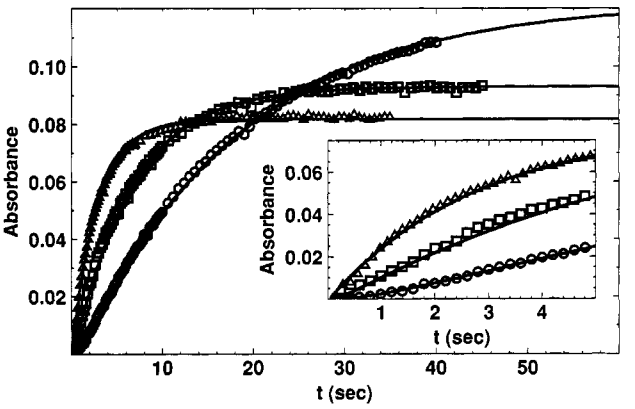

FIGURE 10: Progress curves for the reaction of SLO^A with DHBN. (△) pH 8.1, λ = 680 nm. (□) pH 7.5, λ = 670 nm. (○) pH 6.6, λ = 660 nm. (—) Least squares fits of eq 6 to the data.

be calculated for models with specific numbers of N and O ligands (fits D3−D5), all assumed to have the same bond length. The BVS is 3.7 for seven coordination (e.g., fit D3), well above the allowable range for ferric complexes. Thus, the bond lengths obtained by EXAFS analysis imply six-coordinate iron in SLO^A·DHBN.

Fit D5 differs from D4 in assuming two nitrogen ligands, rather than the three found in the crystal structures of ferrous lipoxygenase (Boyington et al., 1993; Minor et al., 1993). Although EXAFS analysis cannot definitively distinguish nitrogen from oxygen scatterers, fit D5 is more likely to reflect the true coordination because it gives a somewhat lower residual and a BVS closer to the mean for crystallographically characterized high-spin ferric complexes.[2]

The EXAFS amplitude factors we use include contributions for vibrational disorder; thus, the refined $(\Delta\sigma^2)^{1/2}$ is an estimate of the standard deviation of the equilibrium bond lengths (the static disorder in bond lengths) (Scarrow et al., 1994). An alternative approach to modeling the static disorder of bond lengths is to fix $\Delta\sigma^2 \equiv 0$ and to refine individual bond lengths. In practice, least squares refinement with this approach is unfruitful due to high correlations among the six bond lengths. However, we have tested several such models that include shells of two or more atoms at the same bond length. Fits D6 and D7 are representative of such fits. Fits with either two or three Fe−N bonds were obtained; for all good fits, the average refined bond length is 2.03−2.04 Å, the standard deviation of the bond lengths is 0.06−0.08 Å, and BVS = 3.1, in accord with the single shell fits. However, many possible distributions of bond lengths with these characteristics are not consistent with the EXAFS. For instance, if the model of fit D6—two shorter and four longer bonds—is changed to four shorter and two longer bonds, R^2 quadruples and the fit to the Fourier-filtered EXAFS is no longer within the estimated error above $k = 7$ Å^{-1} (Figure 7b). All of the good multiple shell fits with $\Delta\sigma^2 \equiv 0$ show two Fe−O bonds of 1.94 Å (as in fit D6) or one Fe−O bond of 1.92 Å (as in fit D7), with remaining bond lengths clustered close to the average of all bond lengths.

Effects of pH. The absorption maximum of the longer wavelength catechol-to-iron charge transfer band shifts to lower energy as the pH is raised (Figure 8). In addition, the line shapes of the EPR spectra change significantly, with the individual features becoming substantially less resolved as the pH is increased (Figure 9). The latter is consistent with an increase in *E/D*, the rhombicity parameter, as the pH is increased.

Kinetics of Complex Formation. A typical time course of the appearance of the long wavelength absorption of SLO^A·DHBN is shown in Figure 10. For each value of pH and initial concentration of catechol (cat_0), ten such traces were obtained. Those with obvious glitches were eliminated, leaving in each case at least six progress curves to be analyzed individually.

These progress curves could be fitted adequately with a single exponential function, as would result from a mechanism with a single rate-determining step:

$$A + cat \underset{k_2}{\overset{k_1}{\rightleftharpoons}} B \tag{2}$$

$$B = B_{eq}(1 - e^{-\alpha t}) \tag{3}$$

$$\alpha = k_1 cat_0 + k_2 \tag{4}$$

A is SLO^A, cat is the catechol in the reaction, and B_{eq} is the concentration of the complex at equilibrium. In all experiments, cat_0 was much greater than the concentration of SLO^A. However, plots of α vs cat_0 were nonlinear, showing saturation at high concentrations of catechol, a result inconsistent with the postulated single step reaction. Further, samples at low pH and low catechol concentrations (where the reaction is slowest) showed a lag in the progress curves at short times (Figure 10, inset). Consequently, we inferred that the reaction comprises more than one kinetically distinct step.

Therefore, we next assumed we were observing formation of a final complex (C) via an intermediate (B) that was not detected directly in the stopped-flow experiments. In the general case, both steps in such a mechanism may be reversible:

$$A + \text{cat} \underset{k_2}{\overset{k_1}{\rightleftharpoons}} B \underset{k_4}{\overset{k_3}{\rightleftharpoons}} C \quad (5)$$

The general solution to the integrated rate equation for this system is (Connors, 1990)

$$C(t) = C_{eq}\left(1 + \frac{\beta}{\alpha - \beta}e^{-\alpha t} + \frac{\alpha}{\beta - \alpha}e^{-\beta t}\right) \quad (6)$$

$$C_{eq} = C(\infty) = \frac{A_0}{1 + \frac{k_4}{k_3}\left(1 + \frac{k_2}{k_1 \text{cat}_0}\right)} \quad (7)$$

A_0 is the concentration of SLO^A at $t = 0$, and α and β are functions of the microscopic rate constants and cat_0 (see Appendix).

The individual stopped-flow traces (the progress curves for the appearance of C) were fitted separately by eq 6, and average values for α, β, and C_{eq} ($\pm$ standard deviation) were obtained for each value of pH and cat_0. The standard deviations in the average values of β and C_{eq} were generally less than 5%, but α could not be determined with precision. Nevertheless, in all cases, α was at least 10β, leading to (see Appendix)

$$\beta \approx \frac{k_2k_4 + k_1(k_3 + k_4)\text{cat}_0}{k_1\text{cat}_0 + k_2 + k_3 + k_4} \quad (8)$$

Fitting β vs cat_0 with eq 8 gave reasonable estimates of k_1 and $k_3 + k_4$; these values for both DHBN and DHAP are plotted as a function of pH in Figure 11a,b.

At sufficiently high concentrations, C_{eq} is expected to become independent of the concentration of catechol:

$$C_{eq} = \frac{A_0}{1 + \frac{k_4}{k_3}} \quad (9)$$

This was borne out experimentally. The value of C_{eq} (in absorbance units) at high catechol concentrations is plotted in Figure 11c as a function of pH. The decrease in C_{eq} at higher pH is consistent with an increase in the ratio of k_4 to k_3 above pH 7.5.

Complex Formation Is Reversible. The reversibility of complex formation was assessed in a trapping experiment. Pyrocatechol is an efficient reductant of ferric lipoxygenase (Kemal et al., 1987; Nelson, 1988a); visible spectra taken short times after addition of pyrocatechol to ferric lipoxygenase show that the formation of the iron–pyrocatechol complex precedes reduction of the iron (M. J. Nelson, unpublished). Consequently, reduction of SLO^A·DHBN by pyrocatechol can only occur after dissociation of the DHBN from the ferric ion:

$$C \underset{k_3}{\overset{k_4}{\rightleftharpoons}} B \underset{k_1\text{cat}}{\overset{k_2}{\rightleftharpoons}} A(Fe^{3+}) \xrightarrow{k_5P} A(Fe^{2+}) + sq^- \quad (10)$$

where P is the pyrocatechol and sq^- is the oxidized catechol (a semiquinone) [the semiquinone product has been shown to escape from the enzyme (Van der Zee et al., 1989)]. At sufficiently high concentrations of pyrocatechol, $k_5P \gg k_1$cat, any enzyme from which the catechol has dissociated will be trapped by reaction with the pyrocatechol. Under these conditions

$$C(t) = C_0e^{-k_2k_4t/(k_2 + k_3 + k_4)} \quad (11)$$

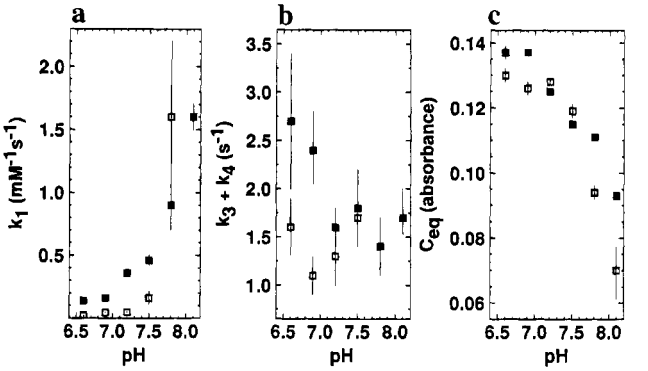

FIGURE 11: Calculated rate constants for the reaction of DHBN and DHAP with ferric lipoxygenase. (■) DHBN. (□) DHAP.

A 100-fold excess of pyrocatechol was added to an anoxic solution of ferric lipoxygenase containing a substoichiometric amount of DHBN. Both the long wavelength catechol-to-iron charge transfer band and the 350 nm absorption band associated with the ferric ion diminished slowly, demonstrating that the lipoxygenase–catechol complexes do indeed spontaneously dissociate. The time courses of the disappearance of both features in the visible spectrum were fitted well by the same single exponential function, showing that the rate of the reduction of the ferric ion was limited by the dissociation of the substituted catechol. In addition, control experiments in which uncomplexed SLO^A was reduced by pyrocatechol under the same conditions verified that the reduction was much faster than the dissociation of the catechols. The values of $k_2k_4/(k_2 + k_3 + k_4)$ obtained were as follows: for DHBN at pH 6.6, 0.0038 $\pm$ 0.0007 s^{-1}; for DHBN at pH 7.2, 0.0045 $\pm$ 0.0014 s^{-1}; for DHBN at pH 8.1, 0.0051 $\pm$ 0.0012 s^{-1}; for DHAP at pH 6.6, 0.0055 $\pm$ 0.0003 s^{-1}; for DHAP at pH 7.2, 0.0092 $\pm$ 0.0008 s^{-1}; and for DHAP at pH 8.1, 0.011 $\pm$ 0.001 s^{-1}.

DISCUSSION

In this study, we have used catechols as probes of the reactivity of the active site iron in lipoxygenase. Our goal was to examine the ability of the metal ion to exchange ligands and expand its coordination sphere as a test of dioxygenase mechanisms that invoke ligation of intermediates to the metal ion. In doing this, we also have developed models for the mechanism of formation and the structure of the lipoxygenase–catechol complexes.

Structure of SLO^A·DHBN. The resonance Raman data demonstrate that DHBN forms a bidentate catecholate complex with the iron in SLO^A, confirming a prediction based on visible spectroscopy (Cox et al., 1988). Considering the similarity among the spectroscopic features of the various lipoxygenase–catechol complexes, it seems likely that all of the catechols examined bind similarly. No crystal structure for SLO^A has been published; nevertheless, CD, MCD, and X-ray spectroscopies (Zhang et al., 1991; Van der Heijdt et al., 1992; Scarrow et al., 1994) agree that the ferric ion in the native enzyme is six-coordinate. The X-ray edge intensity and BVS analysis of the EXAFS of SLO^A·DHBN indicate unambiguously that the DHBN complex is

also six-coordinate. Thus, reaction of ferric lipoxygenase with catechols leads to replacement of two native ligands with catecholate oxygens.

Three lines of evidence from the EXAFS analysis suggest that DHBN displaces a histidine ligand from SLO^A. R^2 decreases by 20% when the ligand set in SLO^A·DHBN is modeled by four O and two N ligands rather than by three O and three N. The BVS is also closer to the expected value of 3.0 when four oxygen and two nitrogen ligands are assumed. Neither of these arguments definitively rules out the possibility of coordination by three O and three N donor ligands. However, if all three histidine ligands in SLO^A (Figure 1) remain coordinated in SLO^A·DHBN, it is reasonable to assume they retain the facial geometry seen in the crystal structure of SLO^N (Boyington et al., 1993; Minor et al., 1993). In that case, both oxygens of the bidentate catecholate ligand would be *trans* to Fe−N bonds. In a series of pseudo-octahedral ferric complexes containing one bidentate catecholate ligand, Que and co-workers found lengths of 1.89−1.92 Å for Fe−O(cat) bonds when *trans* to Fe−N bonds; for instance, in $[Fe(TPA)DBC]^+$, the Fe−O bond lengths are 1.90 and 1.92 Å (Que et al., 1987; Cox & Que, 1988; Jang et al., 1991). On the other hand, Fe−O(cat) bonds *trans* to oxygen ligands have lengths of about 1.98 Å in these complexes. The multishell refinements of EXAFS of SLO^A·DHBN with $\Delta\sigma^2 \equiv 0$ allow at most one Fe−O bond in the 1.89−1.92 Å range (as in fit D7). Thus, the bond length distributions implied by the EXAFS suggest that only one of the catecholate Fe−O bonds is *trans* to Fe−N and therefore that one histidine ligand dissociates when DHBN binds to SLO^A. Our model thus predicts one Fe−O(cat) *trans* to N at about 1.92 Å and one Fe−O(cat) *trans* to O at about 1.98 Å, consistent with fit D7 and the model compound structures. The EXAFS fits also imply that the four non-catecholate Fe−X bond lengths are at least 1.99 Å.

EXAFS and EPR studies of SLO^A (Scarrow et al., 1994; Nelson, 1988b) showed a hydroxide ligand bound to the iron in SLO^A. One of the non-catecholate ligands bound to the iron in SLO^A·DHBN is also either water or hydroxide, as revealed by the line broadening in EPR spectra of samples prepared with $H_2{}^{17}O$. The magnitude of the line broadening of the $g \approx 9.6$ peak, approximately 0.4 mT, is close to that observed in the analogous feature in EPR spectrum of protocatechuate 3,4-dioxygenase in similarly enriched $H_2{}^{17}O$ (Whittaker & Lipscomb, 1984). In that case, a single hydroxide is coordinated to the active site ferric ion (True et al., 1990; Ohlendorf et al., 1994). $Fe^{3+}-OH^-$ or $Fe^{3+}-OH_2$ bonds are about 1.9 Å (Gorun et al., 1987) or 2.04−2.20 Å [for example, Kennedy et al. (1985)], respectively; because all of the bond lengths <1.99 Å in the multishell fits are assigned to Fe−O(cat) bonds (see above), it appears that water, rather than hydroxide, is coordinated in SLO^A·DHBN. Protonation of the hydroxide upon DHBN binding is consistent with replacement of two neutral iron ligands in SLO^A by the anionic catecholate oxygens, decreasing the Lewis acidity of the ferric ion and increasing the pK_a of the hydroxide ligand.

Thus, we conclude that the ferric ion in the lipoxygenase−catechol complexes is coordinated by two histidine imidazoles, one carboxylate, one water, and the bidentate catecholate. As additional support for this model, we note that it is consistent with the prediction, based on electronic spectroscopy, of three neutral ligands and one anionic ligand, in addition to the catecholate, in lipoxygenase−catechol complexes (Cox et al., 1988). It also fits within the framework of the crystal structure of the ferrous enzyme (Minor et al., 1993), if one assumes that one histidine imidazole and the asparagine carboxamide are displaced by the catechol.

It is interesting to compare the six-coordinate catecholate complexes formed by lipoxygenase as well as by tyrosine hydroxylase (Michaud-Soret et al., 1995), to the five-coordinate catecholate−ferric ion complexes formed by the intradiol catechol dioxygenases. The difference in structure correlates with the difference in reactivity; lipoxygenase and tyrosine hydroxylase form stable complexes with catechols in the presence of dioxygen, whereas catechol dioxygenases, with an open coordination site at the metal ion in the catecholate complex, catalyze the catechol ring-opening reaction (Lipscomb & Orville, 1992).

pH Dependence of the Lipoxygenase−Catechol Complexes. The low-energy ligand-to-metal charge transfer band in the visible spectra of lipoxygenase−catechol complexes moves to lower energy as the pH is raised above 7.5. The most likely explanation is that the polarity of the catechol binding site changes with pH. The electronic spectra of ferric catecholate model complexes are sensitive to solvent polarity; in aprotic solvents, the more polar the solvent, the lower the energy of the ligand-to-metal charge transfer band (Cox et al., 1988). A second possibility, however, is that the pH dependence results from a hydrogen bond ($pK_a \approx 7.5$) to the 4-substituent of the catechol.[3] The presence of such a hydrogen bond would effectively increase the electron-withdrawing power of the substituent, resulting in an increase in energy of the ligand-to-metal charge transfer band at lower pH. Supporting this idea is the observation that the visible spectrum of SLO^A·TFMC is significantly less pH-dependent than that of the other catechol complexes; the trifluoromethyl group of TFMC is the weakest hydrogen bond acceptor of the substituents studied. However, we were unable to obtain direct evidence for a pH-dependent hydrogen bond by resonance Raman spectroscopy. We did not observe a resonance-enhanced nitrile stretch in spectra of SLO^A·DHBN at pH 7, and high-fluorescence background prevented spectra of samples prepared at pH 7.5 or above from being obtained.

Interpretation of the Kinetics of the Complexation Reaction. The forward rate of the first kinetically distinct step of the reaction, k_1, increases at higher pH for both DHBN and DHAP. This is inconsistent with a dissociative reaction in which the leaving ligand is protonated to facilitate its dissociation (e.g., $L_5Fe-OH + H^+ \rightarrow L_5Fe-OH_2 \rightarrow L_5Fe$) which should be faster at lower pH. The pH dependence of k_1 is consistent with the catecholate monoanion being a better substrate for the first step of the reaction than the neutral catechol. The pH range over which k_1 increases includes the first pK_a of the catechols studied [DHBN, 7.7; DHAP, 7.8 (Rosenblatt et al., 1953)]. An alternate explanation is that the increase in k_1 at higher pH reflects a general change in structure and reactivity in the active site as the pH is raised

[3] Another obvious possibility is deprotonation of the water ligand above pH 7.5 to yield a hydroxide. However, it was shown in a series of model complexes that the catechol-to-iron charge transfer bands move to higher energy, rather than lower, upon substitution of anionic ligands for neutral ones (Cox et al., 1988a).

from 7 to 8, perhaps the same change that is reflected in the visible and EPR spectra of the final catechol complexes. Changes in the structure of the iron site in this pH range also are reflected in EPR spectra of both the native ferric enzyme (Slappendel et al., 1982; Gaffney et al., 1993) and the nitric oxide complex of ferrous lipoxygenase (Nelson, 1987).

The kinetic data imply the existence of at least one discrete intermediate, B, in the mechanism of the complexation reaction. The reversibility of the complexation reaction ($k_4 \neq 0$) leads to the possibility that an observable amount of B exists in samples prepared with saturating concentrations of DHBN or DHAP. The EPR spectra of such samples contain a new signal, at $g \approx 8.1$, that represents an $S = {}^5/_2$ species not seen in the absence of catechols.

Assuming that this new EPR spectrum arises from the intermediate B, it reflects either a change in the iron structure preceding coordination, possibly a five-coordinate iron species induced by the binding of DHBN to the enzyme in a "Michaelis" complex, or a catechol−iron species distinct from the final complex. An example of the latter would be a monodentate catechol complex, a logical intermediate of the reaction. A model complex, Fe(salen)catH, has a catechol-to-iron charge transfer absorption at 450−500 nm with a long tail to lower energy (Heistand et al., 1982). We did not see conclusive evidence for a contribution from such a band to the visible spectra of the SLO^A·DHBN samples, but the breadth of the absorption features and the relatively small amount of B expected (<20% on the basis of EPR) would make detecting it difficult. Further, resonance Raman spectra of SLO^A·DHBN prepared at pH 7.5, where the $g = 8.1$ signal is most intense, showed no evidence for any species other than the bidentate complex. However, at 714 nm, the excitation wavelength, the visible spectrum of the bidentate complex would be much more intense than that of the monodentate complex, and we would expect the relative resonance enhancement of the monodentate species to be small. At higher excitation energies, where we expect greater resonance enhancement of the monodentate species, the intense fluorescence background did not allow observation of resonance Raman data from SLO^A·DHBN at pH 7.5. Consequently, we have no direct evidence as to the structure of this species.

On the basis of these results and assumptions, a model of the catechol complexation reaction is presented in Figure 12. The starting point, A, is the model of the ferric site in SLO^A in Figure 1. The first step is addition of catecholate monoanion to the enzyme. This could form a Michaelis complex (path 1), with the catecholate in the active site but not coordinated to the iron, or it could form a monodentate iron−catechol complex (path 2). Note that neither of these structures would be expected to have absorption at the wavelength of light used to monitor the stopped-flow experiments. Those experiments only detected the appearance of the final complex; the existence of the intermediate is inferred from the analysis of the progress curves.

The first catechol oxygen is assumed to displace the asparagine from the iron because the O-bonded amide is presumed to be the weakest ligand to the metal ion. The EXAFS data suggest that the second catechol oxygen displaces one of the histidine imidazoles. We propose that this occurs with concomitant proton transfer from the catechol hydroxyl to the leaving imidazole. This is similar

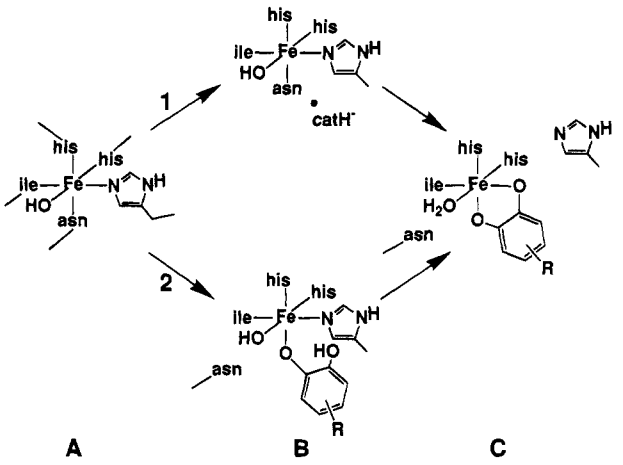

FIGURE 12: Hypothetical mechanisms for the lipoxygenase−catechol coordination reaction. Path 1 predicts the intermediate B is a noncovalent complex. Path 2 predicts B is a monodentate iron−catechol complex.

to the reaction proposed for the second ligation of protocatechuate to the ferric ion in 3,4-protocatechuate dioxygenase, in which the proton is thought to be transferred from the second hydroxyl to the leaving tyrosine phenoxide (Ohlendorf et al., 1994).

Implications for the Function of Lipoxygenase. One of the primary unanswered questions about the mechanism of lipoxygenase is whether substrates, intermediates, or the product coordinates the metal ion at any step. These studies have confirmed that there are at least two labile coordination sites on the iron, but the rate of formation of the catecholate complex, limited to approximately 1−2 s^{-1} at saturating catechol concentration, is much slower than the turnover number of the lipoxygenase dioxygenase reaction, approximately 300 s^{-1}. There is, however, no evidence to suggest that the mechanisms of ligand substitution by catechols and the fatty acid intermediate would be the same. In fact, the putative substrate binding site seen in the crystal structure of SLO^N is adjacent to the site where it is likely that hydroxide binds in SLO^A, suggesting the hydroxide would be displaced in any dioxygenase intermediate complex. However, SLO^A·DHBN includes an aqueous ligand bound to the ferric ion, implying that the hydroxide/water is not displaced during coordination of the catechols. Thus, the ligand exchange chemistry that occurs during catechol complex formation may not be representative of any that might take place during the dioxygenase reaction, and the rates of the catechol reactions may not be directly relevant to a mechanistic step that involves coordination of a dioxygenase intermediate to the metal ion.

In summary, we have shown that catechols form bidentate complexes with the ferric ion in the active site of soybean lipoxygenase isozyme 1, in which the metal ion has a total of six ligands. A histidine imidazole appears to be one of the two native ligands displaced by the catecholate. The hydroxide ligand in the native enzyme is retained and protonated to yield a water ligand in the catecholate complex. The mechanism of complex formation includes an intermediate that may be the monodentate species. EPR and visible spectra of the lipoxygenase−catecholate complexes are sensitive to pH-induced changes in the active site that are consistent with an increase in polarity as the pH is raised.

ACKNOWLEDGMENT

We thank Professor L. Que, Jr., in whose lab the initial resonance Raman spectra were obtained, for a critical reading of the manuscript. We also thank him and Steven Cramer for the loan of equipment used for X-ray spectroscopy.

APPENDIX

Rate Expressions.

$$A + \text{cat} \underset{k_2}{\overset{k_1}{\rightleftharpoons}} B \underset{k_4}{\overset{k_3}{\rightleftharpoons}} C \tag{a1}$$

Here, A is the native ferric lipoxygenase and cat is the catechol in the reaction. The general solutions to the integrated rate equations for this system are (Connors, 1990)

$$A(t) = A_0\left[\frac{k_2k_4}{\alpha\beta} + \frac{k_1(\alpha - k_3 - k_4)}{\alpha(\alpha - \beta)}e^{-\alpha t} + \frac{k_1(\beta - k_3 - k_4)}{\beta(\beta - \alpha)}e^{-\beta t}\right] \tag{a2}$$

$$B(t) = k_1\text{cat}_0A_0\left[\frac{k_4}{\alpha\beta} + \frac{k_4 - \alpha}{\alpha(\alpha - \beta)}e^{-\alpha t} + \frac{k_4 - \beta}{\beta(\beta - \alpha)}e^{-\beta t}\right] \tag{a3}$$

$$C(t) = k_1\text{cat}_0k_3A_0\left[\frac{1}{\alpha\beta} + \frac{1}{\alpha(\alpha - \beta)}e^{-\alpha t} + \frac{1}{\beta(\beta - \alpha)}e^{-\beta t}\right] \tag{a4}$$

$$\alpha = \frac{1}{2}(k_1\text{cat}_0 + k_2 + k_3 + k_4) \times \left[1 + \sqrt{1 - \frac{4[k_2k_4 + k_1(k_3 + k_4)\text{cat}_0]}{(k_1\text{cat}_0 + k_2 + k_3 + k_4)^2}}\right] \tag{a5}$$

$$\beta = \frac{1}{2}(k_1\text{cat}_0 + k_2 + k_3 + k_4) \times \left[1 - \sqrt{1 - \frac{4[k_2k_4 + k_1(k_3 + k_4)\text{cat}_0]}{(k_1\text{cat}_0 + k_2 + k_3 + k_4)^2}}\right] \tag{a6}$$

where A_0 and cat_0 are the total concentration of ferric lipoxygenase and catechol, respectively. At equilibrium ($t = \infty$), the concentration of the final complex is

$$C(\infty) = C_{eq} = \frac{k_1k_3\text{cat}_0A_0}{\alpha\beta} = \frac{k_1k_3\text{cat}_0A_0}{k_2k_4 + k_1(k_3 + k_4)\text{cat}_0} = \frac{A_0}{1 + \frac{k_4}{k_3}\left(1 + \frac{k_2}{k_1\text{cat}_0}\right)} \tag{a7}$$

Note that eq a6 may be expanded as an infinite series:

$$\beta = \frac{1}{2}(k_1\text{cat}_0 + k_2 + k_3 + k_4) + \left(1 - 1 + \frac{z}{2} - \frac{z^2}{8} + \frac{z^3}{32} - \ldots\right) \tag{a8}$$

$$z = \frac{4[k_2k_4 + k_1(k_3 + k_4)\text{cat}_0]}{(k_1\text{cat}_0 + k_2 + k_3 + k_4)^2}$$

and that

$$\frac{\alpha}{\beta} = \frac{1 + \sqrt{1 - z}}{1 - \sqrt{1 - z}}$$

When $\alpha/\beta = 10$, $z \approx {}^1/_3$. Because $(\delta/\delta z)/(\alpha/\beta) < 0$ for all allowed values of z, α/β monotonically decreases between $z = 0$ ($\alpha/\beta = \infty$) and $z = 1$ ($\alpha/\beta = 0$). In every experiment, $\alpha/\beta \geq 10$; thus, $z \leq {}^1/_3$, and eq a8 may be truncated after the first-order term:

$$\beta \approx \frac{1}{2}(k_1\text{cat}_0 + k_2 + k_3 + k_4)\left(1 - 1 + \frac{z}{2}\right) \tag{a9}$$

$$\beta \approx \frac{k_2k_4 + k_1(k_3 + k_4)\text{cat}_0}{k_1\text{cat}_0 + k_2 + k_3 + k_4} \tag{a10}$$

REFERENCES

Blumberg, W. E. (1967) in *Magnetic Resonance in Biological Systems* (Ehrenberg, A., Malmström, B. G., & Vänngard, T., Eds.) pp 119−133, Pergamon Press, Oxford.

Boyington, J. C., Gaffney, B. J., & Amzel, L. M. (1993) *Science (Washington, D.C) 260*, 1482−1486.

Brown, I. D., & Altermatt, D. (1985) *Acta Crystallogr., Sect. B 41*, 244−247.

Clay, K. L., & Murphy, R. C. (1980) *Biomed. Mass Spectrom. 7*, 345−348.

Cohen, T., Dietz, A. G., Jr., & Miser, J. R. (1977) *J. Org. Chem. 42*, 2053−2058.

Connors, K. A. (1990) *Chemical kinetics: the study of reaction rates in solution*, VCH Publishers, New York.

Corey, E. J., & Nagata, R. (1987) *J. Am. Chem. Soc. 109*, 8107−8108.

Cox, D. D., & Que, L., Jr. (1988) *J. Am. Chem. Soc. 110*, 8085−8092.

Cox, D. D., Benkovic, S. J., Bloom, L. M., Bradley, F. C., Nelson, M. J., Que, L., Jr., & Wallick, D. E. (1988) *J. Am. Chem. Soc. 110*, 2026−2032.

De Groot, J. J. M. C., Veldink, G. A., Vliegenthart, J. F. G., Boldingh, J., Wever, R., & Van Gelder, B. F. (1975) *Biochim. Biophys. Acta 377*, 71−79.

Funahashi, S., Ishihara, K., & Tanaka, M. (1983) *Inorg. Chem. 22*, 2070−2073.

Gaffney, B. J., & Silverstone, H. J. (1993) in *Biological Magnetic Resonance* (Berliner, L. J., & Reuben, J., Eds.) pp 1−58, Plenum Press, New York.

Gaffney, B. J., Mavrophilipos, D. V., & Doctor, K. S. (1993) *Biophys. J. 64*, 773−783.

Galpin, J. R., Tielens, L. G. M., Veldink, G. A., Vliegenthart, J. F. G., & Boldingh, J. (1976) *FEBS Lett. 69*, 179−182.

Gardner, H. W. (1991) *Biochim. Biophys. Acta 1084*, 221−239.

Gorun, S. M., Papaefthymious, G. C., Frankel, R. B., & Lippard, S. J. (1987) *J. Am. Chem. Soc. 109*, 4244−4255.

Grant, M., & Jordan, R. B. (1981) *Inorg. Chem. 20*, 55−60.

Heistand, R. H., Lauffer, R. B., Fikrig, E., & Que, L., Jr. (1982) *J. Am. Chem. Soc. 104*, 2789−2796.

Jang, H. G., Cox, D. D., & Que, L., Jr. (1991) *J. Am. Chem. Soc. 113*, 9200−9204.

Kemal, C., Louis-Flamberg, P., Krupinski-Olsen, R., & Shorter, A. (1987) *Biochemistry 26*, 7064−7072.

Kennedy, B. J., Brain, G., Horn, E., Murray, K. S., & Snow, M. R. (1985) *Inorg. Chem. 24*, 1647−1653.

Ling, J. S., Sahlin, M., Sjoberg, B. M., Loehr, T. M., & Sanders-Loehr, J. (1994) *J. Biol. Chem. 269*, 5595−5601.

Lipscomb, J. D., & Orville, A. M. (1992) in *Metal Ions in Biological Systems* (Sigel, H., & Sigel, A., Eds.) Vol. 28, pp 243–298, Marcel Dekker, New York.

Michaud-Soret, I., Andersson, K. K., Que, L., Jr., & Haavik, J. (1995) *Biochemistry 34*, 5504–5510.

Minor, W., Steczko, J., Bolin, J. T., Otwinowski, Z., & Axelrod, B. (1993) *Biochemistry 32*, 6320–6323.

Nelson, M. J. (1987) *J. Biol. Chem. 262*, 12137–12142.

Nelson, M. J. (1988a) *Biochemistry 27*, 4273–4278.

Nelson, M. J. (1988b) *J. Am. Chem. Soc. 110*, 2985–2986.

Nelson, M. J., Cowling, R. A., & Seitz, S. P. (1994) *Biochemistry 33*, 4966–4973.

Ohlendorf, D. H., Orville, A. M., & Lipscomb, J. D. (1994) *J. Mol. Biol. 244*, 586–608.

Orville, A. M., & Lipscomb, J. D. (1989) *J. Biol. Chem. 264*, 8791–8801.

Pilbrow, J. R. (1990) *Transition Ion Electron Paramagnetic Resonance*, Clarendon Press, Oxford.

Pyrz, J. W., Roe, A. L., Stern, L. J., & Que, L., Jr. (1985) *J. Am. Chem. Soc. 107*, 614–620.

Que, L., Jr., & Epstein, R. M. (1981) *Biochemistry 20*, 2545–2549.

Que, L., Jr., Kolanczyk, R. C., & White, L. S. (1987) *J. Am. Chem. Soc. 109*, 5373–5380.

Roe, A. L., Schneider, D. J., Mayer, R. J., Pyrz, J. W., Widom, J., & Que, L., Jr. (1984) *J. Am. Chem. Soc. 106*, 1676–1681.

Rosenblatt, D. H., Epstein, J., & Levitch, M. (1953) *J. Am. Chem. Soc. 75*, 3277–3278.

Scarrow, R. C., Trimitsis, M. G., Buck, C. P., Grove, G. N., Cowling, R. A., & Nelson, M. J. (1994) *Biochemistry 33*, 15023–15035.

Siedow, J. N. (1991) *Annu. Rev. Plant Physiol. Plant Mol. Biol. 42*, 145–188.

Slappendel, S., Veldink, G. A., Vliegenthart, J. F. G., Åasa, R., & Malmström, B. G. (1981) *Biochim. Biophys. Acta 667*, 77–86.

Slappendel, S., Åasa, R., Malmström, B. G., Verhagen, J., Veldink, G. A., & Vliegenthart, J. F. G. (1982) *Biochim. Biophys. Acta 708*, 259–265.

Stevenson, G. R., Wang, Z. Y., Reiter, R. C., & Peters, S. J. (1988) *J. Am. Chem. Soc. 110*, 6581–6582.

Swaddle, T. W., & Merbach, A. E. (1981) *Inorg. Chem. 20*, 4212–4216.

Thompson, L. K., Ramaswamy, B. S., & Seymour, E. A. (1977) *Can. J. Chem. 55*, 878–888.

Thorpe, H. H. (1992) *Inorg. Chem. 31*, 1585–1588.

True, A. E., Orville, A. M., Pearce, L. L., Lipscomb, J. D., & Que, L., Jr. (1990) *Biochemistry 29*, 10847–10854.

Van der Heijdt, L. M., Feiters, M. C., Navaratnam, S., Nolting, H.-F., Hermes, C., Veldink, G. A., & Vliegenthart, J. F. G. (1992) *Eur. J. Biochem. 207*, 793–802.

Van der Zee, J., Eling, T. E., & Mason, R. P. (1989) *Biochemistry 28*, 8363–8367.

van Eldik, R., Cohen, H., & Meyerstein, D. (1994) *Inorg. Chem. 33*, 1566–1568.

Whittaker, J. W., & Lipscomb, J. D. (1984) *J. Biol. Chem. 259*, 4487–4495.

Zhang, Y., Gebhard, M. S., & Solomon, E. I. (1991) *J. Am. Chem. Soc. 113*, 5162–5175.

BI951307R